Journal of
Low Power Electronics and Applications

MDPI

Review

Key Role of Cold-Start Circuits in Low-Power Energy Harvesting Systems: A Research Review

Xiao Shi, Mengye Cai and Yanfeng Jiang *

School of Integrated Circuits, Jiangnan University, Wuxi 214122, China; 6221916008@stu.jiangnan.edu.cn (X.S.); caimengye@jiangnan.edu.cn (M.C.)
* Correspondence: jiangyf@jiangnan.edu.cn

Abstract: The primary functions of an energy harvesting system include the harvesting, transformation, management, and storage of energy. Until now, various types of energy, with different power levels, have been harvested and stored by the energy harvesting system. In low-power scenarios, such as microwaves, sound, friction, and pressure, a specific low-power energy harvesting system is required. Due to the absence of an external power supply in such systems, cold-start circuits play a crucial role in igniting the low-power energy harvesting system, ensuring a reliable start-up from the initial state. This paper reviews the categorization and characteristics of energy harvesting systems, with a focus on the design and performance parameters of cold-start circuits. A tabular comparison of existing cold-start strategies is presented herein. The study demonstrates that resonance-based integrated cold-start methods offer significant advantages in terms of conversion efficiency and dynamic range, while ring oscillator-based integrated cold-start methods achieve the lowest start-up voltage. Additionally, the paper discusses the challenges of self-starting and future research directions, highlighting the potential role of emerging technologies, such as artificial intelligence (AI) and neural networks, in optimizing the design of energy harvesting systems.

Keywords: low-power energy harvesting system; cold-start circuit; LC resonant; ring oscillator

check for updates

Citation: Shi, X.; Cai, M.; Jiang, Y. Key Role of Cold-Start Circuits in Low-Power Energy Harvesting Systems: A Research Review. *J. Low Power Electron. Appl.* **2024**, *14*, 55. https://doi.org/10.3390/jlpea14040055

Received: 1 October 2024
Revised: 9 November 2024
Accepted: 19 November 2024
Published: 22 November 2024

Copyright: © 2024 by the authors. Licensee MDPI, Basel, Switzerland. This article is an open access article distributed under the terms and conditions of the Creative Commons Attribution (CC BY) license (https://creativecommons.org/licenses/by/4.0/).

1. Introduction

The number and diversity of microelectronic products are growing rapidly due to advances in science and technology, which play an essential role in the Internet of Things (IoT), biosensors, microelectromechanical systems (MEMSs), and portable electronic devices, etc. The rapid expansion of microelectronic systems has lead to a sharp rise in energy consumption, which severely affects the delicate balance between power provision and energy usage. Additionally, this increased energy consumption negatively affects the environment [1].

Recently, energy harvesting technology has been proposed to collect and store previously untapped sources of environmental energy. The harvested energy can be stored and be applied to specific appliances, such as human body implanted devices and sensor networks without an energy supply [2,3]. Energy sources for harvesting include piezoelectric, triboelectric, electromagnetic, electrostatic, thermoelectric, and light/solar energy [4]. To convert the above-mentioned scattered energy into stored electrical energy, different approaches can be applied. For example, electrostatic, triboelectric, and electromagnetic energy can be converted by frictional contact. Piezoelectric methods employ active materials to convert mechanical strain into electrical energy. Heat generated from industrial production [5] or human activity [6] is also an important source of energy harvesting. In addition, a design method for capacitor-based energy harvesting systems has been proposed that utilizes switches to implement a pulsed harvesting system, maximizing the utilization efficiency of the storage capacitor during transients, making it functional for radio frequency energy harvesting (RFEH) applications [7]. In summary, the diversity of

these energy harvesting strategies presents complex systematic considerations for their design in order to meet whole system requirements in different scenarios.

In a stand-alone energy harvesting system, the absence of an external power supply means the entire system operates passively, fully relying on the harvested environmental energy to activate the system. Therefore, the autonomous start-up of energy harvesting systems presents a critical challenge. To address this issue, specialized start-up circuits and power management strategies should be designed deliberately to minimize energy consumption during start-up.

Currently, various cold-start circuits have been developed to initiate systems with ultra-low voltage. However, in the research community there is lack of a systematic classification and comprehensive comparison of proposed cold-start circuits with different operation modes. In the review, a systematic classification of cold-start circuits is summarized. The key characteristics and performances of different cold-start circuits are discussed, which can be helpful for choosing a suitable cold-start strategy for specific application scenarios.

The paper is organized as follows: the energy harvesting systems are presented in the second part, the operational principles of low-power energy harvesting-based cold-start circuits are discussed in the third part, and the characteristics of cold-start circuits are reviewed in the paper.

2. Classification of Energy Harvesting Systems

Energy harvesting technology can be used to capture tiny scattered amounts of energy from surrounding sources and store it in the designed energy harvesting system. Hopefully, the technology can be treated as a possible solution for novel batteries, which can be automatically charged with an unlimited lifetime. Such batteries offer significant advantages over traditional batteries in certain applications. For example, in a sensor network, a huge number of batteries are required to provide the power needed by the active sensors. However, these batteries have a limited lifespan, leading to high-frequency replacement and maintenance [8]. In this context, a novel battery based on an energy harvesting system offers advantages in practical applications. With advancements in wireless and MEMS technologies, energy harvesting is considered a viable alternative to conventional batteries, offering longer lifespans, reduced maintenance, and higher power efficiency. Consequently, energy harvesting technology is regarded to be a self-power source for wearable devices and wireless sensors.

Research has demonstrated that energy harvesting systems can capture energy from various widely available sources, including solar, vibration, electromagnetic (RF), and thermal energy, as illustrated in Figure 1.

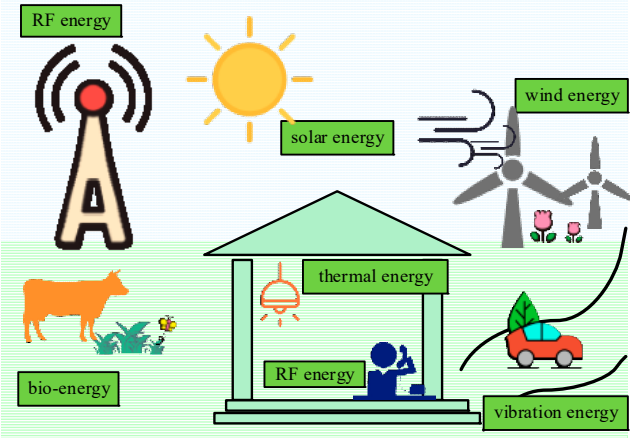


Figure 1. Energy sources in life environment.

Many studies have demonstrated various approaches to converting vibrational energy into the electrical power [1,3,9–11]. Piezoelectric energy harvesting is effective in converting

mechanical energy into electrical energy and is more reliable than triboelectric energy harvesting [12,13]. As shown in Figure 2, the coupling relationship between the electrical and mechanical components of a piezoelectric energy harvester can be modeled as an ideal transformer, with the left side of the transformer representing the mechanical part, while the right side, apart from the internal capacitor Cp of the transducer, represents the electrical circuit load.

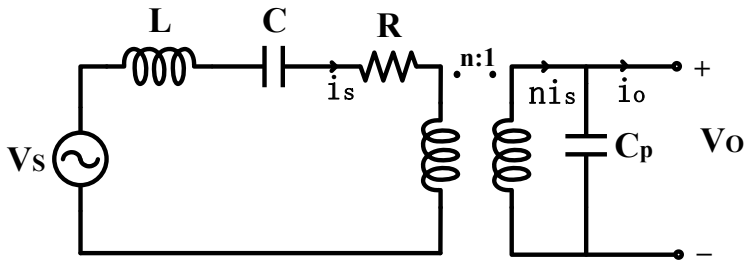


Figure 2. Equivalent electrical model of the piezoelectric energy harvester.

This equivalent electrical model also satisfies the fundamental laws of electricity:

$$\begin{cases} V_S = L\frac{di_s}{dt} + Ri_s + \frac{1}{C}\int i_s dt + nV_0 \\ i_O = ni_s - C_P\frac{dV_0}{dt} \end{cases} \quad (1)$$

Therefore, circuit simulation can be conducted to analyze the performance of a piezoelectric transducer, facilitating the design and validation of the piezoelectric interface circuit. To enhance its performance, various types of piezoelectric materials have been tested in energy harvesting systems, including thin films, laminated layers, and nanostructures. Compared to other techniques, the output power of piezoelectric generators is at least three to five times higher [13–17]. Furthermore, piezoelectric generators are unaffected by environmental variables, and can be feasibly embedded in micro-electro-mechanical systems (MEMSs) [18–22]. Thus, piezoelectric technology is widely considered as a highly promising approach for energy harvesting, with extensive applications in various domains including wearable technology, transportation, and implanted biomedical devices [23–27].

Thermal energy is extensively employed in remote power applications [28,29], where the Seebeck effect and the Poincaré effect are utilized for power conversion, as shown in Figure 3. When there is a temperature difference across the substrate of the TEG, holes in the p-type semiconductor and electrons in the n-type semiconductor move from the hot side to the cold side, creating a voltage difference ΔV between the metal electrodes:

$$\Delta V = S \times (T_H - T_C) \quad (2)$$

where S is the relative Seebeck coefficient, and T_H and T_C are the substrate temperatures at the hot side and cold side, respectively.

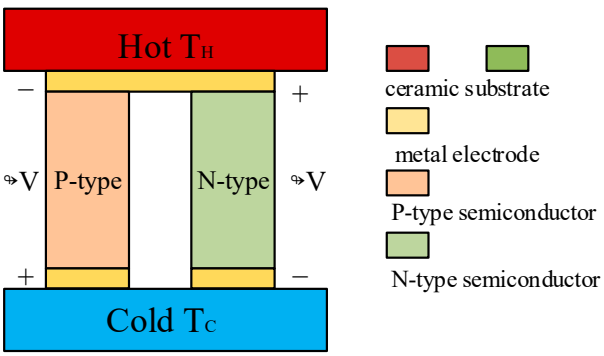


Figure 3. Schematic diagram of Seebeck effect.

As shown in Figure 4, the equivalent electrical model of a thermoelectric generator (TEG) can be represented as a voltage source with a certain internal resistance. When there is a temperature gradient, a current is generated. At room temperature, the power density with the human body as a heat source ranges from 20 mW/cm^2 to 60 mW/cm^2 [30]. Thermoelectric energy harvesting systems provide several advantages, including high dependability, quasi-static operation, and environmental sustainability. However, their efficiency is low and the generated power is significantly constrained.

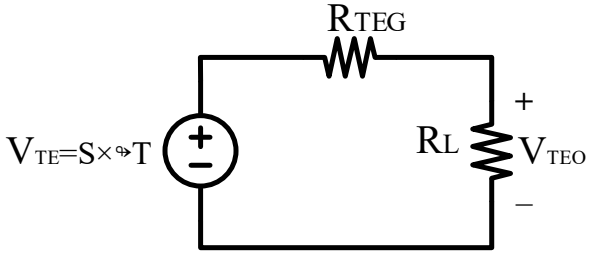


Figure 4. Equivalent electrical model of TEG.

Common renewable energy sources such as wind and solar power are widely regarded as clean energy alternatives. Wind energy has dominated the clean energy market for many years. In contrast, solar energy has shown a rapid growth in energy collection in recent years [31,32]. Photovoltaic panels are the main devices used for power conversion [33]. The produced electrical energy is managed and collected by the solar harvesting circuit.

Figure 5 shows the equivalent circuit model of a solar energy harvesting circuit. In this model, Ui represents the equivalent voltage of the photovoltaic cell and Ri represents its equivalent internal resistance. The circuit can be operated in two states, depending on the state of the switch transistor VT1. With VT1 in the on state, the energy is stored in the inductor L. In the off state, the stored energy in L is forcibly transferred to the storage capacitor C. With the periodic switching operation, the electrical energy from the photovoltaic cell is periodically transferred via inductor L to capacitor C, thereby achieving solar energy harvesting.

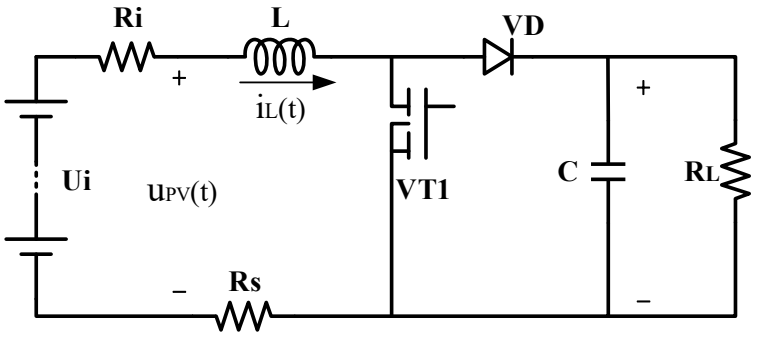


Figure 5. Equivalent electrical model of solar energy harvesting.

Hiyama T. et al. demonstrated the significance of environmental factors in determining the cost and efficiency of energy harvesting systems [34,35]. For instance, during the daytime, solar energy has an average power density of nearly 100 mW/cm^2 [36]. However, its efficiency is decreased at night or in cloudy conditions [37]. Solar energy systems perform sub-optimally in winter or at high latitudes. Wind energy systems also exhibit limited productivity at low wind speeds and are less effective in regions with consistently low wind speeds.

RFEH involves the harvesting of scattered RF signals from the environment, such as those emitted by cell phones, Wi-Fi, and Bluetooth. The harvested RF signals can be transferred into electrical energy. RF energy is a form of electromagnetic energy. Figure 6

shows the equivalent electrical model of RFEH, where R_A represents the impedance of the antenna, RF is the RF energy harvested by the antenna, and $Z_N = R_N + jX_N$ is the input impedance of the rectifier circuit. Code S. et al. demonstrated that RF signals within the 3 kHz to 3 GHz band can be used to transfer electromagnetic energy from a transmitting source to a receiver, exemplifying a typical use case for RF energy harvesting. Compared to other energy harvesting systems, RFEH systems may provide relatively consistent and readily available energy. To ensure network stability and long-term viability, Ren J. et al. presented the online algorithm JAMA [38], which automatically adapts to channel characteristics including sampling rate, transmitted power, transmission rate, and channel assignment. Concurrently, Ren J. et al. studied RF energy harvesting and transmission in cognitive radio sensor networks (CRSNs) [39], a method that offers a durable, energy-efficient, and spectrum-efficient wireless network solution.

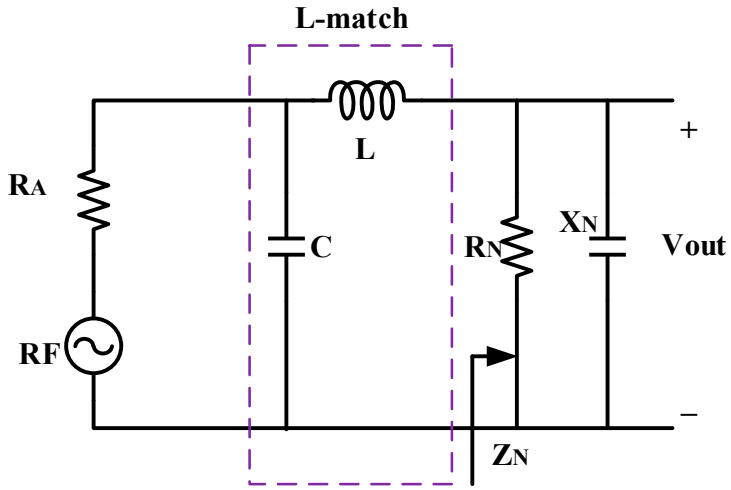


Figure 6. Equivalent electrical model of RFEH.

The coverage of popular energy sources and power consumption levels is shown in Figure 7. It indicates that a wide variety of consumer electrical devices are operated at the micro-watt power consumption level. In this context, RF energy harvesting systems may serve as a power supply for portable electronics.

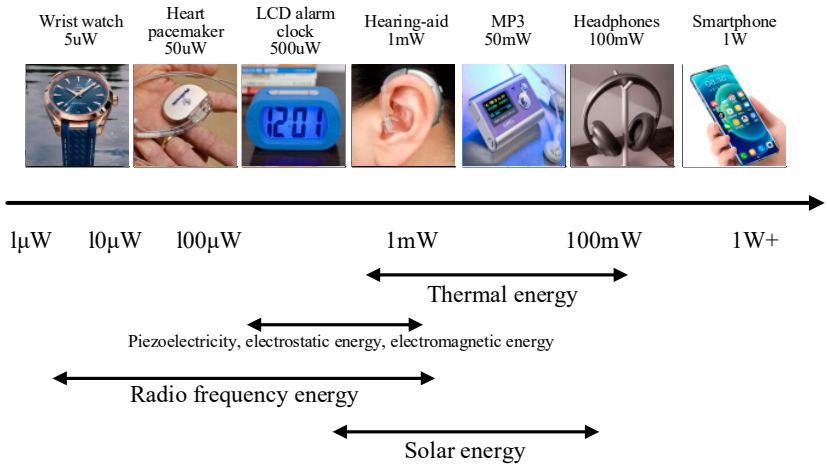


Figure 7. Typical device power consumption of consumer electronics.

Table 1 lists the power densities and attributes of the four previously discussed energy sources [40]. In comparison, RF energy offers the advantages of low cost and ease of application.

Table 1. Power densities and energy characteristics of four types of energy sources.

		Electric Energy	Voltage Size	Energy Source Power Density	Collected Power Density
Thermal energy	Civil	DC voltage	0–1 V	0.1 mW/cm^2	10 μW/cm^2
	Industry			100 mW/cm^2	10 mW/cm^2
Solar energy	Indoor	DC voltage	>0.7 V	0.1 mW/cm^2	4 μW/cm^2
	Outdoor			100 mW/cm^2	100 μW/cm^2
Vibration energy	Civil	Pulse voltage	1–100 V	0.5 m@1 Hz, 1 m/s^2 @50 Hz	30 μW/cm^2
	Industry			1 m@5 Hz, 10 m/s^2 @1 KHz	1–10 μW/cm^2
RF energy	Environment	Sinusoidal voltage	0–1 V	20 W/cm^2	0.1 μW/cm^2
	Emission source			0.3 μW/cm^2	0.1 μW/cm^2

A multi-source energy system integrates various harvested energy sources, combining their advantages, as illustrated in Figure 8. By utilizing multiple energy sources, the multi-source energy harvesting strategy can enhance energy utilization efficiency.

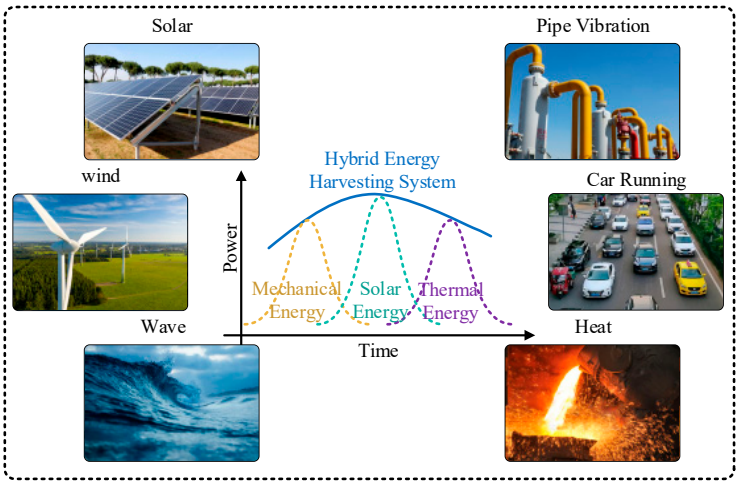


Figure 8. Schematic of hybrid energy harvesting system.

In 2020, Wang XD et al. investigated the simultaneous extraction of energy from a thermoelectric generator (TEG) and a piezoelectric transducer (PZT) [41]. The researchers designed a hybrid self-powered synchronous charge extraction circuit using double-stacked resonance. The output power of the circuit can exceed three times the maximum power point achieved by a conventional full-bridge rectifier (FBR) circuit. In 2023, a multi-source synergistic energy extraction (MSC-EC) circuit was proposed by Shi G. et al. [42], in which TEG, PZT, and photovoltaic (PV) energies were harvested simultaneously. The three energy sources are stored collaboratively in a capacitor. The MSC-EC employs non-time-division multiplexing architecture and utilizes a single inductor, minimizing the size and effectively addressing energy efficiency issues.

3. Cold-Start Circuit

To ensure the effective operation of the power management unit (PMU), a cold-start circuit is required in the energy harvesting system to generate an initial clock signal at ultra-low input voltages. As shown in Figure 9, the designed energy harvesting system collects and converts external energy into electrical energy. The main components include the energy converter, PMU, and the cold-start circuit. The cold-start circuit generates an oscillating clock under low-voltage conditions without any external power supply. With

the clock signal generated by the cold-start circuit under extreme low-voltage conditions, the PMU and other parts of the system can be started up. Following the start-up phase, the energy harvesting system can be ignited to start the harvesting operation. Various cold-start methods are reviewed in this paper. These methods are categorized into two main groups: discrete cold-start methods [43–50] and integrated cold-start methods [51–58].

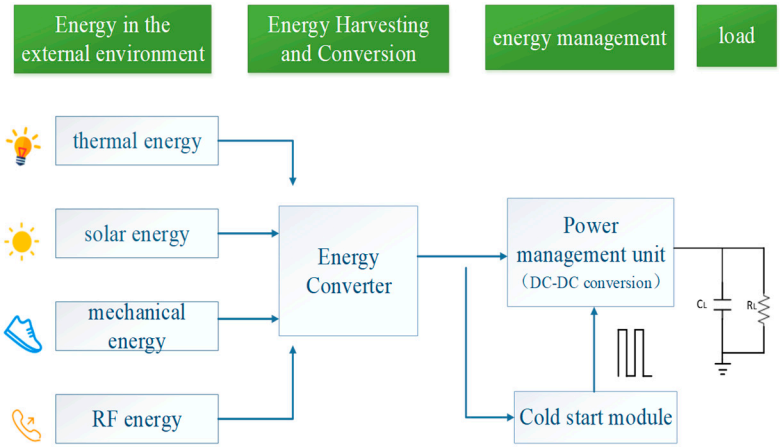


Figure 9. Cold-start module in an energy harvesting system.

3.1. Discrete Cold-Start Component

The three main methods for cold-start using discrete components are transformer-based, LC oscillator-based, and MEMS switch-based.

Figure 10 shows the MEMS switch-based cold-start technique, which operates under low-power and low-voltage conditions. This approach does not rely on any external power sources or conventional batteries. It adopts microscopic switching elements S1 to respond to specific stimuli, such as mechanical displacements (vibrations). In 2011, Ramadass, YK suggested a thermoelectric energy harvesting system for wearable devices [59]. The system utilized MEMS switches that harnessed human limb movements as signals, achieving a cold-start voltage as low as 35 mV.

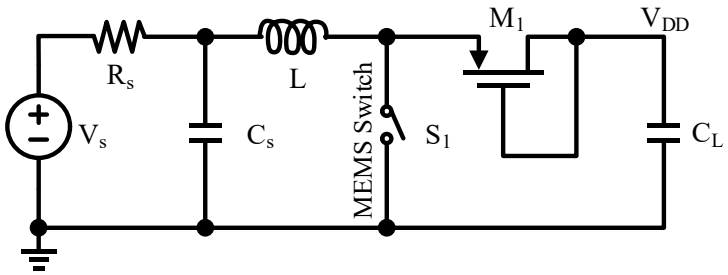


Figure 10. Cold-start scheme based on MEMS switches [59].

Figure 11 shows a transformer-based cold-start method, suitable for starting a circuit under low-voltage or energy-limited circumstances. The transformer effectively increases the input voltage. In 2012, Im J. P. et al. proposed a transformer-based self-starting step-up converter structure [43]. The transformer performs as a start-up element during the initial phase. After the initial phase, the transformer could be operated as an inductor for standard boosting operations, effectively reducing the initial cold-start voltage and enhancing the overall conversion efficiency. In 2014, Teh Y.-K. et al. proposed an improved boost converter based on a miniature pulse transformer [60]. It was demonstrated that setting the transformer turns ratio to 1:1 constitutes the most significant enhancement to this system, as it reduces the impact of parasitic capacitance and eliminates the impedance transformation multiplier effect. However, the integration of the transformer is challenging,

and the discrete transformer inevitably reduces the voltage conversion efficiency in energy harvesting applications.

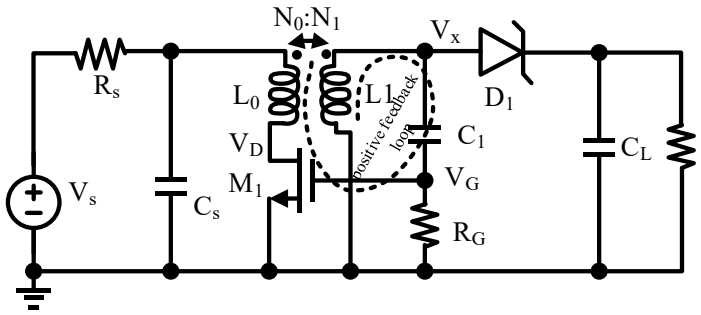


Figure 11. Transformer-based cold-start scheme [60].

Figure 12 illustrates a cold-start circuit employing the LC oscillation method, wherein the LC oscillator operates in a resonant state. Mok Philip et al. proposed an energy harvesting system that is capable of simultaneously managing discrete and continuous energy sources [44]. The core DC-DC converter, acting as a pulse transformer boost converter, is capable of self-starting at an input voltage of 36 mV. Additionally, although the LC oscillator-based cold-start method can initiate the system at a low voltage, MOS devices are operated in depletion mode, thereby increasing the circuit complexity. Furthermore, the addition of external inductive devices reduces the system's compactness. Therefore, selecting a cold-start solution requires careful consideration of all relevant factors.

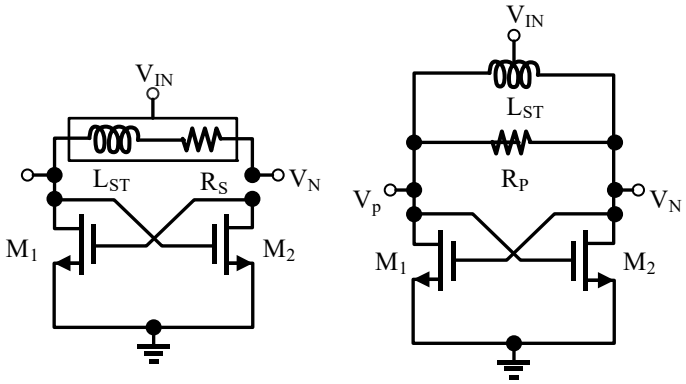


Figure 12. Cold-start scheme based on LC oscillator circuit [44].

3.2. Integrated Cold-Start Approaches

Although the aforementioned methods can be operated at ultra-low voltages, obvious disadvantages still exist. Furthermore, despite some success in integrating transformers and inductors on-chip, issues related to insertion loss and chip size still remain in the system design. Extensive studies have been conducted on fully integrated solutions.

Generally, evaluating the performance of cold-start circuits requires several key parameters, including start-up voltage, start-up time, conversion efficiency, dynamic range, and immunity to interference, as listed in Table 2. For harvesting systems, a low start-up voltage is essential to ensure proper operation even under low-voltage and unstable power conditions. To enhance user experience and responsiveness, engineers have designed systems to minimize the start-up time for various applications. An optimized cold-start circuit should exhibit high conversion efficiency to minimize wasted power, thereby extending battery life and reducing energy costs. Furthermore, the dynamic range of the cold-start circuit needs to be sufficiently wide to account for inevitable variations in voltage and power. The most critical aspect is the anti-interference capability, which is used as the key parameter for evaluating the stability and reliability of the cold-start procedure.

Table 2. Key parameters of cold-start circuits.

Parameter	Interpretation	Unit
Starting voltage	Minimum voltage required for cold-start of equipment or system	V
Starting time	The time interval between the initial start-up signal being delivered to the circuit and the circuit being able to function properly and perform its designed function	ms
Output frequency	The frequency of the generated oscillating signal usually needs to be compatible with subsequent circuits	Hz
Dynamic range	Voltage range in which the cold-start circuit can operate	
Anti-interference	The ability to operate normally when the equipment or system is subjected to external interference	

Fully integrated cold-start strategies can be categorized into three groups: ring oscillator-based, self-excited oscillation-based, and resonance-based cold-starts.

3.2.1. Integrated Ring Oscillator-Based Cold-Start Approach

Recently, ring oscillator-based cold-start systems for energy harvesting have garnered significant attention. However, due to the fragility of their power supply and susceptibility to MOS device noise, this approach has not achieved widespread adoption.

To stabilize the ring oscillator and ensure compatibility with standard CMOS technology, researchers have constructed them using an intrinsic transistor [48]. In 2015, Ashraf et al. suggested a comprehensive energy-harvesting power supply for implantable pacemakers, as shown in Figure 13 [61]. A forward body bias reduces the initial activation voltage of the ring oscillator, enabling the circuit to be started at 60 mV. Unfortunately, operating the ring oscillator across different process corners has proven unfeasible. In 2018, Dezyani M. et al. introduced a thermoelectric energy harvesting system featuring a new process-tolerant inverter unit [53], implemented as a ring oscillator in Figure 14. The oscillator incorporates traditional inverters combined with additional circuitry, ensuring successful operation across various process corners. This approach eliminates the need for post-fabrication adjustments or trimming, while remaining compatible with standard CMOS technology. The harvesting system can be operated with an input voltage as low as 60 mV, generating 4.5 µW of output power. Soumya Bose et al. developed a modified ring oscillator architecture, shown in Figure 15 [56]. The input signal V_{in} is amplified to be V_a at node a by the inverter INV1, and is amplified to be Vb at node b by the inverter INV3. The equivalent input signal for M3 is V_{in} (1 + A_1), where A_1 is the gain of the inverter INV1. Similarly, the input signal for M4 is V_{in} (1 + A_3), where A_3 is the gain of inverter INV3. As a result, the effective trans-conductance G_m is

$$G_m = (1 + A_1)g_{m3} + (1 + A_3)g_{m4} \tag{3}$$

The DC gain of each inverter stage is

$$\mathrm{A} = \frac{g_{mN} + g_{mP}}{g_{dsN} + g_{dsP}} \tag{4}$$

A_1 and A_3 are low (≈1) due to the deep sub-threshold operation. Moreover, due to the low intrinsic gains of M3 and M4, the transformed output impedance is primarily dominated by g_{ds3} and g_{ds4}. Therefore, the DC gain of this delay element is

$$\mathrm{A} = \frac{(1 + A_1)g_{m3} + (1 + A_3)g_{m4}}{g_{ds3} + g_{ds4}} \tag{5}$$

This increase in gain enhances the ability of the ring oscillator, constructed with triple-stacked inverter delay elements to start and sustain oscillation at an extremely low supply voltage, enabling it to operate at voltages as low as 50 mV.

The start-up voltage plays a crucial role in the quality assessment of a cold-start circuit. A reduction in start-up voltage would benefit the energy harvesting system. As shown in Figure 16, Z. Xie et al. suggested a novel delay element in 2020 [62], incorporating dynamic body biasing and stacking techniques. This approach enables the ring oscillator to exhibit a wider output voltage range during initial activation.

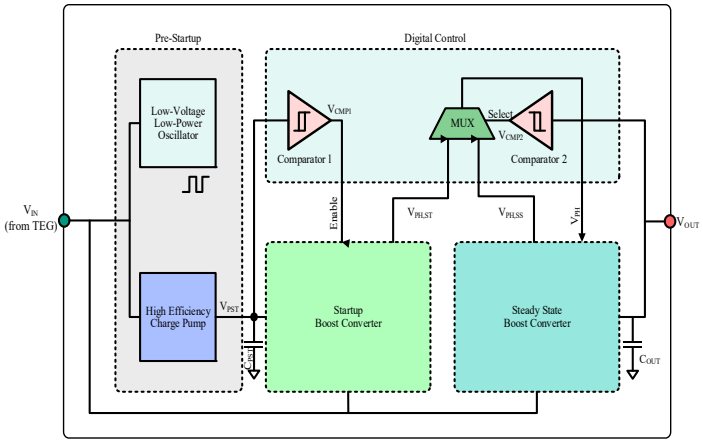


Figure 13. TEG energy harvesting system architecture [61].

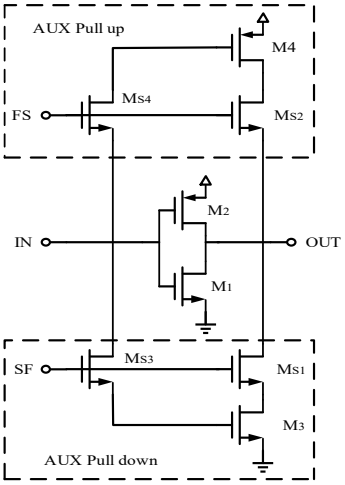


Figure 14. Proposed process-tolerant inverter unit [53].

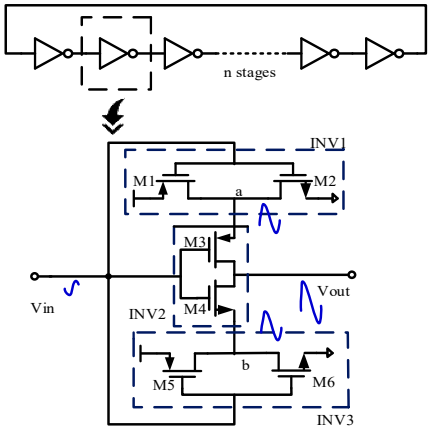


Figure 15. Enhanced ring oscillator configuration featuring a triple-stacked arrangement of inverter delay elements [56].

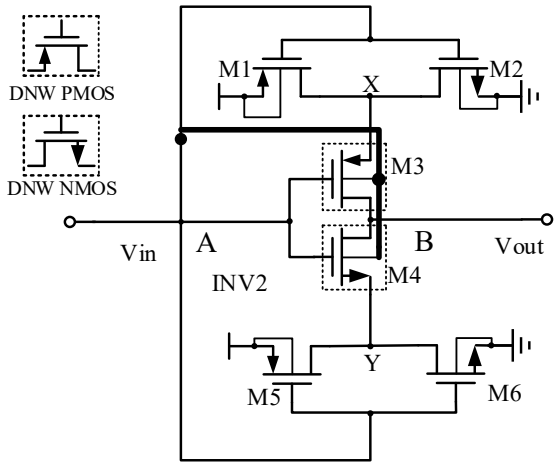


Figure 16. Schematic of low-voltage delay elements [63].

A ring oscillator that is designed to start at low voltages employs dynamically biased delay elements with low-voltage characteristics [63], as shown in Figure 17. A low-voltage level shifter (VLS) increases the range of voltage used to bias the delay element. When the supply voltage drops to 24 mV, the cold-start ring oscillator operates continuously at room temperature. M. Nishi et al. proposed a ring oscillator (ROSC) tailored for thermoelectric energy generators operating at extremely low voltages [64]. As shown in Figure 18, the designed ROSC consists of a stacked inverter (SI) and a conventional self-bias inverter (SBI). For a conventional inverter, the maximum value of the voltage gain |AINV| is

$$|\mathrm{AINV}|_{MAX} = \frac{1}{\eta}\left\{\exp\left(\frac{V_{DD}}{2V_T}\right) - 1\right\} \quad (6)$$

where η and V_T are the sub-threshold slope factor and the thermal voltage, respectively [65].

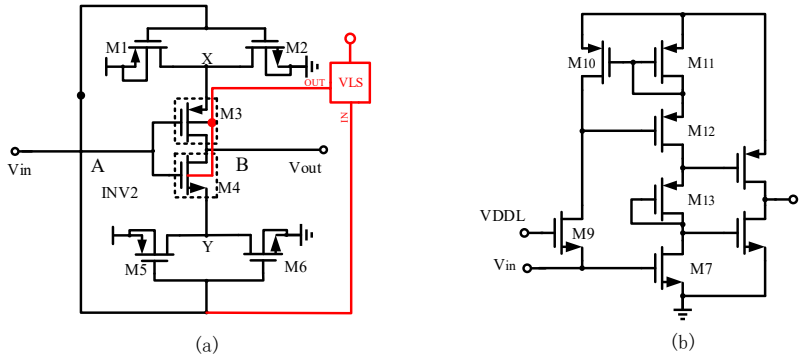


Figure 17. Schematic of (**a**) the proposed delay element (**b**) VLS [63].

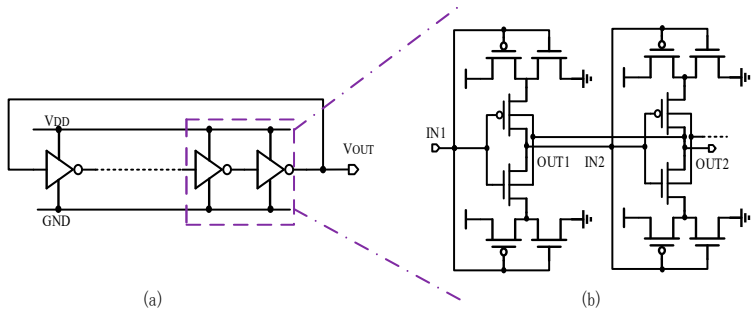


Figure 18. Schematic of (**a**) ROSC (**b**) and two SBBIs [64].

It was found that $|AINV|_{MAX}$ decreases with decreasing VDD. The SI consists of three inverters. By using the additional two inverters, the trans-conductance of the NMOS and PMOS transistors in the main inverter are increased, thereby enhancing the $|AINV|_{MAX}$ of the SI [57]. Therefore, in this study, the low-voltage stacked body bias inverter (SBBI) composed of one SI and one SBI can oscillate at very low voltages. The ROSC generates clock pulses at an input of 50 mV and a VDD of 34 mV, featuring an 88% voltage swing.

In 2023, Z Xie et al. proposed a PMU designed for RF energy harvesting systems, featuring a broad dynamic range and high efficiency [66]. The PMU needs to be started at low incident power. Thus, the cold-start circuit should provide stable voltage and sufficient power to complete the start-up process of the control circuit. The proposed PMU shows a cold-start voltage of 280 mV.

3.2.2. Integrated Resonance-Based Cold-Start

Resonance occurs when a system exhibits the maximum amplitude and the highest energy transfer efficiency, specifically when its operation frequency matches the external excitation frequency. Resonance-based cold-start represents a rapid and effective start-up strategy. This technique can significantly reduce start-up time and energy consumption, thereby enhancing the performance and reliability of the energy harvesting system.

The improved conversion efficiency is crucial for energy harvesting systems, as it reduces energy loss, extends battery life, and enhances system performance. A 95-mV start-up boost converter [51], as shown in Figure 19, was reported by PH Chen et al. in 2011, achieving a conversion efficiency of 72%. Energy harvesting systems based on this technique become more applicable when mechanical switches and external clocks are eliminated. Additionally, the design shows the feasibility of the minimum start-up voltage for the on-chip ring oscillator. In 2012, a dual-mode boost converter for energy harvesting systems was proposed [67], as shown in Figure 20. The converter employs an inductive boost DC-DC converter for both start-up and operational modes, utilizing a charge-pump pulse generator (CPPG) to drive the power transistor. The system can be started with an ultra-low voltage of 80 mV in 4.8 ms. A maximum conversion efficiency of 72% is achieved at an output current of 0.5 mA.

In 2013, Weng, P.-S. et al. proposed an all-electric start-up boost converter for thermal energy harvesting [46], as shown in Figure 21. It features a three-stage boost configuration with a start-up voltage as low as 50 mV. By combining the automated shutdown mechanism of the auxiliary converter with a zero-current switching (ZCS) converter, it achieves a conversion efficiency of up to 73%. In 2017, H. Fuketa et al. proposed a fully integrated boost voltage converter [47], as shown in Figure 22. This converter utilizes an LC oscillator (LCO) as its start-up mechanism, allowing operation with a start-up voltage of 100 mV. To further enhance efficiency, it is recommended to deactivate the gate boost CP and LCO. The converter achieves a conversion efficiency of 33%. To achieve on-chip voltage multiplication at a low input voltage, Soumya Bose et al. proposed an integrated cold-start design, as shown in Figure 23, which adopts a cross-coupled gate boost approach [57]. An ultra-low voltage ring oscillator generates an on-chip clock that regulates the start-up of the voltage multiplier. The one-button start-up mechanism enables the integrated cold-start circuit to boost the converter within 135 ms, with an input voltage as low as 57 mV.

In 2017, Y. Ma et al. introduced a fully integrated self-starting circuit [68] with an exceptionally low input voltage, as shown in Figure 24. The design incorporates a charge pump and an improved swing LC oscillator. When the input voltage fluctuates between 0.2 V and 0.4 V, the maximum efficiency reaches 14.8%. However, the design shows a relatively large layout area due to the inclusion of four on-chip inductors. In 2023, a cold-start circuit with fewer off-chip components was proposed [69], as shown in Figure 25. In this circuit, the inductors and load capacitors are shared with the primary boost converter, eliminating the need for extra off-chip components and resulting in a smaller layout area. Additionally, a fully autonomous multi-input, single-inductor, multi-output energy harvesting platform with power management (EHPMU) was proposed [70]. With a 1-μA

output current, the EHPMU achieves 80% efficiency, a dynamic range of 1.2×10^5, a 3.2× energy extraction gain for piezoelectric energy harvesting, and a static current of 32 nA.

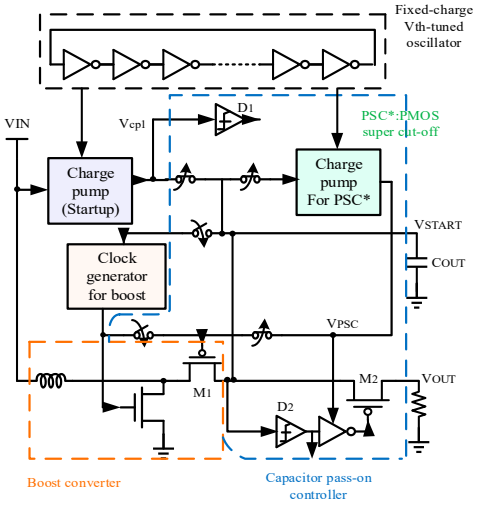


Figure 19. Block diagram of the proposed boost converter [51].

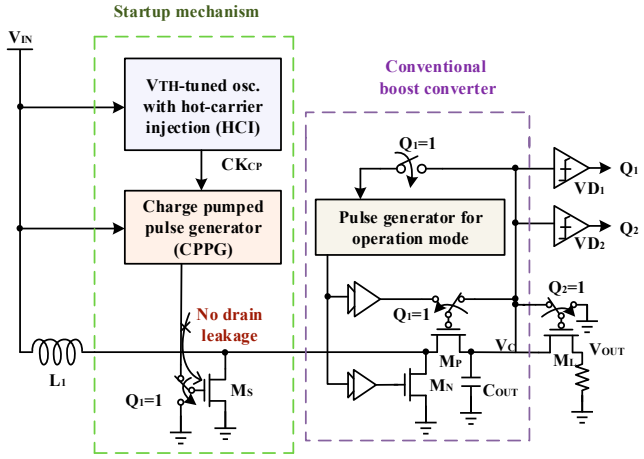


Figure 20. Block diagram of the proposed dual-mode boost converter [67].

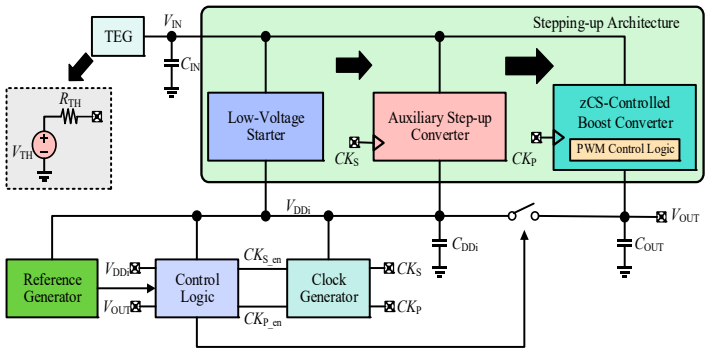


Figure 21. Block diagram of the proposed three-stage stepping-up architecture [46].

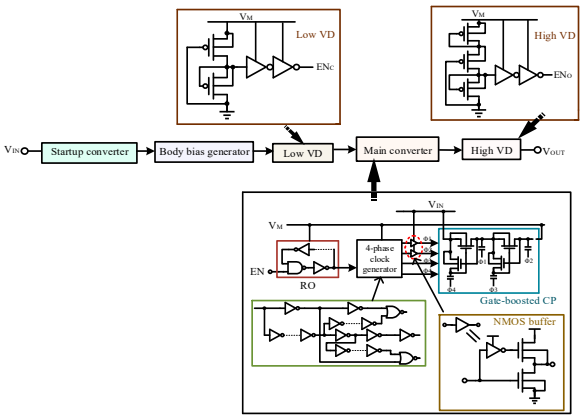


Figure 22. Proposed boost converter schematic [47].

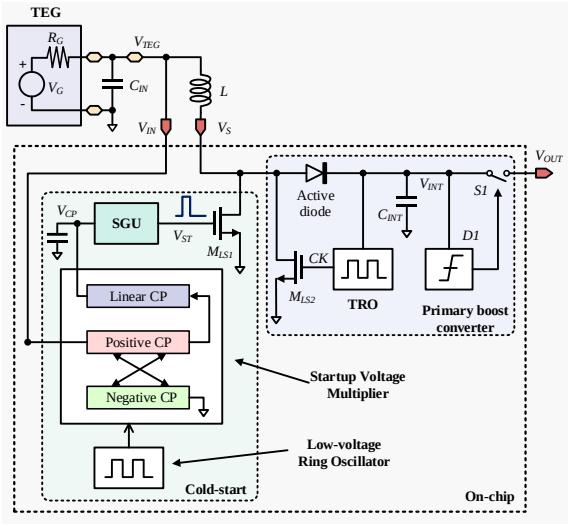


Figure 23. Proposed integrated cold-start architecture [57].

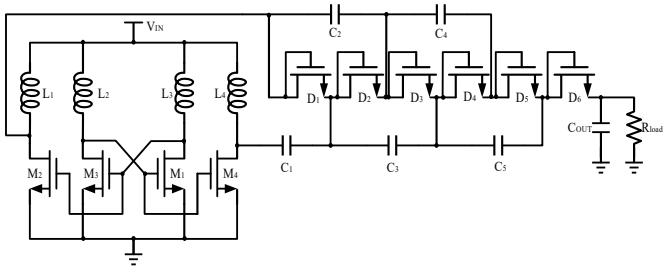


Figure 24. The proposed start-up circuits [68].

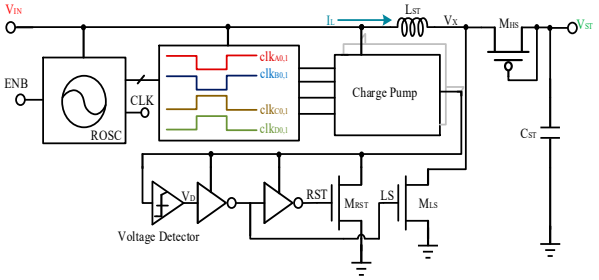


Figure 25. The architecture of the proposed cold-start-up circuit or a thermoelectric [69].

3.2.3. Integrated Self-Excited Oscillation-Based Cold-Start

During the initial system start-up, the nonlinear nature and unstable conditions of the system can result in self-induced oscillation or unexpected fluctuation. Self-excited oscillations can be employed as a cold-start approach; however, they may negatively impact the system's stability. To ensure the system reaches a stable state rapidly, it is essential to thoroughly consider self-induced oscillation during both the start-up and design phases.

In 2017, a study on an inductive power converter in a thermoelectric generator (TEG) was published by Zhihong Luo et al. [54]. A new redundant inverter ring oscillator exhibiting self-excited oscillations at 45 mV was proposed. Additionally, a self-starting auxiliary circuit, which incorporates an exponential charge pump and a differential clock booster, was added to the power converter. This extra circuit generated an operational voltage of 7 mV and a self-starting voltage of 210 mV. In 2019, Mathieu Coustans et al. introduced a novel cold-start method for thermoelectric harvesters [71], as shown in Figure 26. The controller of the single-inductor boost converter is powered by a low-voltage self-oscillating charge pump. Due to its capability to operate at input voltages as low as 60 mV, the converter allows for adjustments based on the process conditions and core temperatures of the chip. This approach can be expanded at the board level, incorporating readily available energy harvesting components to extend the range of the cold-start voltage.

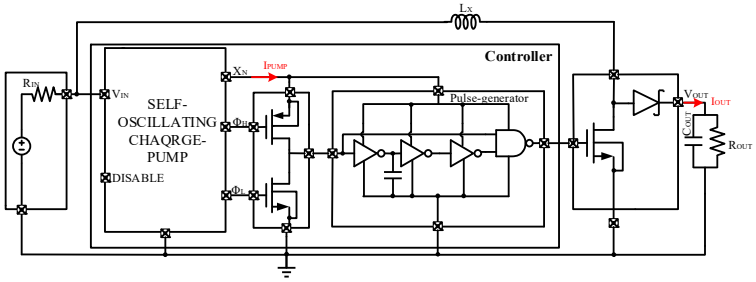


Figure 26. Proposed cold-start circuit architecture [71].

4. Discussion

The self-start-up issue remains a focal point for the future development of energy harvesting systems. With the proliferation of the Internet of Things (IoT) and wireless sensor networks, developing efficient cold-start circuits is essential to ensure stable operation in low-energy environments. Additionally, artificial intelligence (AI) and neural networks can enable adaptive energy management, optimizing energy harvesting and storage strategies to enhance the overall system performance and efficiency. Dotche K. A. et al. proposed a distributed hybrid grid power management method based on artificial neural networks (ANNs) [72], introducing a multi-objective formula to maximize both regional spectrum efficiency and energy efficiency. Regarding the maximum power point tracking (MPPT) algorithm, which is especially crucial for renewable energy systems, Breesam W. I. suggested an AI-based real-time MPPT system designed with an Arduino microcontroller [73]. Neural networks are used to predict the optimal power and rotation speed of a wind turbine, while fuzzy neural networks predict the optimal duty cycle to drive DC-DC converters, allowing maximum power extraction from the solar panels under various temperature and illumination conditions. Overall, AI and neural networks hold great potential for advancing energy management, significantly improving the efficiency of energy harvesting, storage, and utilization.

In future, self-start-up research will integrate AI and neural network technologies to drive the efficient use and intelligent management of renewable energy. Meanwhile, research on novel energy harvesting materials utilizing various physical mechanisms, such as the photovoltaic effect, thermoelectricity, piezoelectricity, triboelectricity, and radiofrequency wireless power transfer, can efficiently convert ambient energy into electrical power [74]. In terms of energy sources, developing multiple ambient energy harvesting so-

lutions can not only enhance the availability of energy but also improve devices' autonomy and reliability, reducing reliance on traditional power sources [75]. Ultimately, by integrating advanced power management and energy harvesting technologies, more efficient and cost-effective autonomous power systems can be designed to provide continuous power support for future smart devices.

5. Conclusions

Energy harvesting technology shows significant potential for wireless sensors and portable devices. It not only reduces costs, but also alleviates the environmental concerns associated with traditional batteries. Cold-start circuits are crucial for ensuring the reliable start-up of energy harvesting systems and efficient capture of ambient energy. This paper reviews the design of cold-start circuits for energy harvesting systems. The key parameters for evaluating the characteristics of cold-start circuits are summarized in Table 2. The comparison of published cold-start strategies and key parameters is presented in Table 3. Among the multiple reported cold-start approaches, the resonance-based integrated cold-start approach shows significant advantages in conversion efficiency and dynamic range, while the ring oscillator-based integrated cold-start circuit achieves the lowest start-up voltage.

Table 3. Comparison index for different cold-start circuits.

Categorization		Reference	Starting Voltage	Starting Time	Peak Efficiency	Dynamic Range	Maximum Output Power	CMOS Process
Non-fully integrated		[43]	40 mV	/	61%	/	2.7 mw	130 nm
		[60]	21 mV	/	74%	/	2 mw	130 nm
		[44]	36 mV	/	/	/	2 mw	130 nm
Fully integrated	Ring oscillator-based	[76]	225 mV	/	/	/	/	180 nm
		[63]	24 mV	/	/	/	/	180 nm
	Resonance-based	[67]	80 mV	4.8 ms	72%	/	/	65 nm
		[57]	57 mV	135 ms	/	/	/	180 nm
		[70]	/	/	80%	1.2×10^5	1.2 mw	65 nm
	Self-excited Oscillation-based	[77]	83 mV	/	81%	/	/	55 nm
		[54]	210 mV	/	71.5%	/	/	65 nm
		[71]	60 mV	150 ms	/	/	/	180 nm

Author Contributions: Conceptualization, Y.J. and X.S.; methodology, X.S.; software, X.S.; validation, X.S., Y.J. and M.C.; formal analysis, X.S.; investigation, M.C.; resources, Y.J.; data curation, X.S.; writing—original draft preparation, X.S.; writing—review and editing, Y.J.; visualization, M.C.; supervision, Y.J.; project administration, M.C.; funding acquisition, Y.J. All authors have read and agreed to the published version of the manuscript.

Funding: This work was funded in part by Leading Technology Pre-Research Project (No.XD23008, Wuxi Industrial Innovation Research Institute and Jiangsu JITRI IC Application Technology Innovation Center), National Natural Science Foundation of China under Grant No.61774078 and Natural Science Foundation of Jiangsu Province (BK20210453).

Data Availability Statement: No new data were created or analyzed in this study.

Conflicts of Interest: On behalf of all authors, the corresponding author states that there are no conflicts of interest.

References

1. Zhou, C.; Yang, Y.; Sun, N.; Wen, Z.; Cheng, P.; Xie, X.; Shao, H.; Shen, Q.; Chen, X.; Liu, Y.; et al. Flexible self-charging power units for portable electronics based on folded carbon paper. *Nano Res.* **2018**, *11*, 4313–4322. [CrossRef]
2. Yahya Alkhalaf, H.; Yazed Ahmad, M.; Ramiah, H. Self-sustainable biomedical devices powered by RF energy: A review. *Sensors* **2022**, *22*, 6371. [CrossRef]

3. Nundrakwang, S.; Yingyong, P.; Isarakorn, D. Energy harvesting for self-powered systems. In Proceedings of the 2020 6th International Conference on Engineering, Applied Sciences and Technology (ICEAST), Chiang Mai, Thailand, 1–4 July 2020; IEEE: Piscataway, NJ, USA, 2020.
4. Evangelakos, E.A.; Kandris, D.; Rountos, D.; Tselikis, G.; Anastasiadis, E. Energy sustainability in wireless sensor networks: An analytical survey. *J. Low Power Electron. Appl.* **2022**, *12*, 65. [CrossRef]
5. Rowe, D.M.; Min, G. Evaluation of thermoelectric modules for power generation. *J. Power Sources* **1998**, *73*, 193–198. [CrossRef]
6. Singh, J.; Kaur, R.; Singh, D. Energy harvesting in wireless sensor networks: A taxonomic survey. *Int. J. Energy Res.* **2021**, *45*, 118–140. [CrossRef]
7. Tampouratzis, M.G.; Plevritakis, N.; Vouyioukas, D.; Yioultsis, T.; Stratakis, D. Storage Efficiency Optimization in Capacitor-based Energy Harvesting Systems. In Proceedings of the 2023 International Conference on Control, Artificial Intelligence, Robotics & Optimization (ICCAIRO), Crete, Greece, 11–13 April 2023; IEEE: Piscataway, NJ, USA, 11–13 April 2023.
8. Zhao, W.; Gadfort, P.; Bhanushali, K.; Franzon, P.D. RF-only logic: An area efficient logic family for RF-power harvesting applications. *IEEE Trans. Circuits Syst. I Regul. Pap.* **2017**, *65*, 406–418. [CrossRef]
9. Hu, D.; Yao, M.; Fan, Y.; Ma, C.; Fan, M.; Liu, M. Strategies to achieve high performance piezoelectric nanogenerators. *Nano Energy* **2019**, *55*, 288–304. [CrossRef]
10. Karan, S.K.; Maiti, S.; Agrawal, A.K.; Das, A.K.; Maitra, A.; Paria, S.; Bear, A.; Bear, R.; Halder, L.; Mishra, A.K.; et al. Designing high energy conversion efficient bio-inspired vitamin assisted single-structured based self-powered piezoelectric/wind/acoustic multi-energy harvester with remarkable power density. *Nano Energy* **2019**, *59*, 169–183. [CrossRef]
11. Yan, J.; Liu, M.; Jeong, Y.G.; Kang, W.; Li, L.; Zhao, Y.; Deng, N.; Cheng, B.; Yang, G. Performance enhancements in poly(vinylidene fluoride)-based piezoelectric nanogenerators for efficient energy harvesting. *Nano Energy* **2019**, *56*, 662–692. [CrossRef]
12. Thainiramit, P.; Yingyong, P.; Isarakorn, D. Impact-driven energy harvesting: Piezoelectric versus triboelectric energy harvesters. *Sensors* **2020**, *20*, 5828. [CrossRef]
13. Sezer, N.; Koç, M. A comprehensive review on the state-of-the-art of piezoelectric energy harvesting. *Nano Energy* **2021**, *80*, 105567. [CrossRef]
14. Chen, J.; Oh, S.K.; Nabulsi, N.; Johnson, H.; Wang, W.; Ryou, J.H. Biocompatible and sustainable power supply for self-powered wearable and implantable electronics using III-nitride thin-film-based flexible piezoelectric generator. *Nano Energy* **2019**, *57*, 670–679. [CrossRef]
15. Fei, C.; Liu, X.; Zhu, B.; Li, D.; Yang, X.; Yang, Y.; Zhou, Q. AlN piezoelectric thin films for energy harvesting and acoustic devices. *Nano Energy* **2018**, *51*, 146–161. [CrossRef]
16. Iqbal, M.; Nauman, M.M.; Khan, F.U.; Abas, P.E.; Cheok, Q.; Iqbal, A.; Aissa, B. Vibration-based piezoelectric, electromagnetic, and hybrid energy harvesters for microsystems applications: A contributed review. *Int. J. Energy Res.* **2021**, *45*, 65–102. [CrossRef]
17. Wu, N.; Bao, B.; Wang, Q. Review on engineering structural designs for efficient piezoelectric energy harvesting to obtain high power output. *Eng. Struct.* **2021**, *235*, 112068. [CrossRef]
18. Shirvanimoghaddam, M.; Shirvanimoghaddam, K.; Abolhasani, M.M.; Farhangi, M.; Barsari, V.Z.; Liu, H. Towards a green and self-powered Internet of Things using piezoelectric energy harvesting. *IEEE Access* **2019**, *7*, 94533–94556. [CrossRef]
19. Brusa, E.; Carrera, A.; Delprete, C. A Review of Piezoelectric Energy Harvesting: Materials, Design, and Readout Circuits. *Actuators* **2023**, *12*, 457. [CrossRef]
20. Zhou, X.; Parida, K.; Halevi, O.; Liu, Y.; Xiong, J.; Magdassi, S.; Lee, P.S. All 3D-printed stretchable piezoelectric nanogenerator with non-protruding kirigami structure. *Nano Energy* **2020**, *72*, 104676. [CrossRef]
21. Sun, Y.; Chen, J.; Li, X.; Lu, Y.; Zhang, S.; Cheng, Z. Flexible piezoelectric energy harvester/sensor with high voltage output over wide temperature range. *Nano Energy* **2019**, *61*, 337–345. [CrossRef]
22. Wu, N.; Derkenne, T.; Tregouet, C.; Colin, A. Comparison of miniaturized mechanical and osmotic energy harvesting systems. *Nano Energy* **2023**, *118*, 109004. [CrossRef]
23. He, Q.; Briscoe, J. Piezoelectric Energy Harvester Technologies: Synthesis, Mechanisms, and Multifunctional Applications. *ACS Appl. Mater. Interfaces* **2024**, *16*, 29491–29520. [CrossRef]
24. Parvez Mahmud, M.; Huda, N.; Farjana, S.H.; Asadnia, M.; Lang, C. Recent advances in nanogenerator-driven self-powered implantable biomedical devices. *Adv. Energy Mater.* **2018**, *8*, 1701210. [CrossRef]
25. Zheng, Q.; Shi, B.; Li, Z.; Wang, Z.L. Recent Progress on Piezoelectric and Triboelectric Energy Harvesters in Biomedical Systems. *Adv. Sci.* **2017**, *4*, 1700029. [CrossRef]
26. Bouhamed, A.; Missaoui, S.; Ben Ayed, A.; Attaoui, A.; Missaoui, D.; Jeder, K.; Guesmi, N.; Njeh, A.; Khemakhem, H.; Kanoun, O. A comprehensive review of strategies toward efficient flexible piezoelectric polymer composites based on $BaTiO_3$ for next-generation energy harvesting. *Energies* **2024**, *17*, 4066. [CrossRef]
27. Yang, D.; Sun, A.; Pan, Y.; Wang, K. Mechanical Energy Harvesting: Advancements in Piezoelectric Nanogenerators. *Int. J. Electrochem. Sci.* **2024**, *19*, 100793. [CrossRef]
28. Rahman, M.M.; Khan, I.; Field, D.L.; Techato, K.; Alameh, K. Powering agriculture: Present status, future potential, and challenges of renewable energy applications. *Renew. Energy* **2022**, *188*, 731–749. [CrossRef]
29. Kumar, C.M.S.; Singh, S.; Gupta, M.K.; Nimdeo, Y.M.; Raushan, R.; Deorankar, A.V.; Kumar, T.M.A.; Rout, P.K.; Chanotiya, C.; Nannaware, A.D.; et al. Solar energy: A promising renewable source for meeting energy demand in Indian agriculture applications. *Sustain. Energy Technol. Assess.* **2023**, *55*, 102905. [CrossRef]

30. Leonov, V. Thermoelectric Energy Harvesting of Human Body Heat for Wearable Sensors. *IEEE Sens. J.* **2013**, *13*, 2284–2291. [CrossRef]
31. Solangi, K.; Islam, M.; Saidur, R.; Rahim, N.A.; Fayaz, H. A review on global solar energy policy. *Renew. Sustain. Energy Rev.* **2011**, *15*, 2149–2163. [CrossRef]
32. Coşgun, A.E.; Demir, H. The experimental study of dust effect on solar panel efficiency. *Politek. Derg.* **2022**, *25*, 1429–1434. [CrossRef]
33. Demir, H. Application of thermal energy harvesting from photovoltaic panels. *Energies* **2022**, *15*, 8211. [CrossRef]
34. Demir, H.; Coşgun, A.E. Performance prediction approach using rainfall based on artificial neural network for PV module. In Proceedings of the International Symposium on Current Developments in Science, Technology and Social Sciences, Gaziantep, Turkey, 16–17 December 2021.
35. Hiyama, T.; Kitabayashi, K. Neural network based estimation of maximum power generation from PV module using environmental information. *IEEE Trans Energy Convers.* **1997**, *12*, 241–247. [CrossRef]
36. Banotra, A.; Mishra, D.; Modem, S. Stochastic Computation Model for Solar Panel Size and Cost of Sustainable IoT Networks. *IEEE Trans. Sustain. Comput.* **2024**, 1–17. [CrossRef]
37. Wang, C.; Li, J.; Yang, Y.; Ye, F. Combining Solar Energy Harvesting with Wireless Charging for Hybrid Wireless Sensor Networks. *IEEE Trans. Mob. Comput.* **2017**, *17*, 560–576. [CrossRef]
38. Ren, J.; Yue, S.; Zhang, D.; Zhang, Y.; Cao, J. Joint channel assignment and stochastic energy management for RF-powered OFDMA WSNs. *IEEE Trans. Veh. Technol.* **2018**, *68*, 1578–1592. [CrossRef]
39. Ren, J.; Hu, J.; Zhang, D.; Guo, H.; Zhang, Y.; Shen, X. RF Energy Harvesting and Transfer in Cognitive Radio Sensor Networks: Opportunities and Challenges. *IEEE Commun. Mag.* **2018**, *56*, 104–110. [CrossRef]
40. Vullers, R.; van Schaijk, R.; Doms, I.; Van Hoof, C.; Mertens, R.M.E.H. Micropower energy harvesting. *Solid-State Electron.* **2009**, *53*, 684–693. [CrossRef]
41. Wang, X.; Xia, Y.; Shi, G.; Xia, H.; Ye, Y.; Chen, Z. Self-powered piezoelectric and thermoelectric energy simultaneous extraction interface circuit based on double stack resonance. *IEEE Trans. Ind. Electron.* **2019**, *67*, 4567–4577. [CrossRef]
42. Shi, G.; Chang, J.; Xia, Y.; Wang, X.; Xia, H.; Li, Q. A Multisource Collaborative Energy Extraction Circuit for Vibration, Ambient Light, and Thermal Energy with MPPT and Single Inductor. *IEEE Trans. Ind. Electron.* **2022**, *70*, 5819–5829. [CrossRef]
43. Im, J.P.; Wang, S.W.; Ryu, S.T.; Cho, G.H. A 40mV transformer-reuse self-startup boost converter with MPPT control for thermoelectric energy harvesting. *IEEE J. Solid-State Circuits* **2012**, *47*, 3055–3067. [CrossRef]
44. Teh, Y.-K.; Mok, P.K. DTMOS-based pulse transformer boost converter with complementary charge pump for multisource energy harvesting. *IEEE Trans. Circuits Syst. II Express Briefs* **2015**, *63*, 508–512. [CrossRef]
45. Tang, H.Y.; Weng, P.S.; Ku, P.C.; Lu, L.H. A fully electrical startup batteryless boost converter with 50mV input voltage for thermoelectric energy harvesting. In Proceedings of the 2012 Symposium on VLSI Circuits (VLSIC), Honolulu, HI, USA, 13–15 June 2012; IEEE: Piscataway, NJ, USA, 2012.
46. Weng, P.S.; Tang, H.Y.; Ku, P.C.; Lu, L.H. 50 mV-Input Batteryless Boost Converter for Thermal Energy Harvesting. *IEEE J. Solid-State Circuits* **2013**, *48*, 1031–1041. [CrossRef]
47. Fuketa, H.; Matsukawa, T. Fully integrated, 100-mV minimum input voltage converter with gate-boosted charge pump kick-started by LC oscillator for energy harvesting. *IEEE Trans. Circuits Syst. II Express Briefs* **2016**, *64*, 392–396. [CrossRef]
48. Machado, M.B.; Schneider, M.C.; Galup-Montoro, C. On the minimum supply voltage for MOSFET oscillators. *IEEE Trans. Circuits Syst. I Regul. Pap.* **2013**, *61*, 347–357. [CrossRef]
49. Rozgic, D.; Markovic, D. A 0.78mW/cm2 autonomous thermoelectric energy-harvester for biomedical sensors. In Proceedings of the 2015 Symposium on VLSI Circuits, Kyoto, Japan, 17–19 June 2015.
50. Rozgić, D.; Markovic, D. A Miniaturized 0.78-mW/cm^2 Autonomous Thermoelectric Energy-Harvesting Platform for Biomedical Sensors. *IEEE Trans. Biomed. Circuits Syst.* **2017**, *11*, 773–783. [CrossRef]
51. Chen, P.H.; Ishida, K.; Ikeuchi, K.; Zhang, X.; Honda, K.; Okuma, Y.; Sakurai, T. A 95mV-startup step-up converter with Vth-tuned oscillator by fixed-charge programming and capacitor pass-on scheme. In Proceedings of the 2011 IEEE International Solid-State Circuits Conference, San Francisco, CA, USA, 20–24 February 2011.
52. Goeppert, J.; Manoli, Y. Fully Integrated Startup at 70 mV of Boost Converters for Thermoelectric Energy Harvesting. *IEEE J. Solid State Circuits* **2016**, *51*, 1716–1726. [CrossRef]
53. Dezyani, M.; Ghafoorifard, H.; Sheikhaei, S.; Serdijn, W.A. A 60 mV input voltage, process tolerant start-up system for thermoelectric energy harvesting. *IEEE Trans. Circuits Syst. I Regul. Pap.* **2018**, *65*, 3568–3577. [CrossRef]
54. Luo, Z.; Zeng, L.; Lau, B.; Lian, Y.; Heng, C.H. A sub-10 mV power converter with fully integrated self-start, MPPT, and ZCS control for thermoelectric energy harvesting. *IEEE Trans. Circuits Syst. I Regul. Pap.* **2017**, *65*, 1744–1757. [CrossRef]
55. Bose, S.; Anand, T.; Johnston, M.L. Fully-integrated 57 mV cold-start of a thermoelectric energy harvester using a cross-coupled complementary charge pump. In Proceedings of the 2018 IEEE Custom Integrated Circuits Conference (CICC), San Diego, CA, USA, 8–11 April 2018.
56. Bose, S.; Johnston, M.L. A Stacked-Inverter Ring Oscillator for 50 mV Fully-Integrated Cold-Start of Energy Harvesters. In Proceedings of the 2018 IEEE International Symposium on Circuits and Systems (ISCAS), Florence, Italy, 27–30 May 2018.
57. Bose, S.; Anand, T.; Johnston, M.L. Integrated Cold-start of a Boost Converter at 57 mV Using Cross-Coupled Complementary Charge Pumps and Ultra-Low-Voltage Ring Oscillator. *IEEE J. Solid-State Circuits* **2019**, *54*, 2867–2878. [CrossRef]

58. Bose, S.; Anand, T.; Johnston, M.L. A 3.5 mV input, 82% peak efficiency boost converter with loss-optimized MPPT and 50 mV integrated cold-start for thermoelectric energy harvesting. In Proceedings of the 2019 IEEE Custom Integrated Circuits Conference (CICC), Austin, TX, USA, 14–17 April 2019; IEEE: Piscataway, NJ, USA, 2019.
59. Ramadass, Y.K.; Chandrakasan, A.P. A battery-less thermoelectric energy harvesting interface circuit with 35 mV startup voltage. *IEEE J. Solid-State Circuits* **2010**, *46*, 333–341. [CrossRef]
60. Teh, Y.K.; Mok, P.K. Design of Transformer-Based Boost Converter for High Internal Resistance Energy Harvesting Sources with 21 mV Self-Startup Voltage and 74% Power Efficiency. *IEEE J. Solid-State Circuits* **2014**, *49*, 2694–2704. [CrossRef]
61. Ashraf, M.; Masoumi, N. A Thermal Energy Harvesting Power Supply With an Internal Startup Circuit for Pacemakers. *IEEE Trans. Very Large Scale Integr. Syst.* **2015**, *24*, 26–37. [CrossRef]
62. Xie, Z.; Wu, Z.; Wu, J. Low voltage delay element with dynamic biasing technique for fully integrated cold-start in DC energy harvesting systems. *AEU-Int. J. Electron. Commun.* **2020**, *127*, 153416. [CrossRef]
63. Xie, Z.; Wu, Z.; Wu, J. Low Voltage Delay Element with Dynamic Biasing Technique for Fully Integrated Cold-Start in Battery-Assistance DC Energy Harvesting Systems. *Appl. Sci.* **2020**, *10*, 6993. [CrossRef]
64. Nishi, M.; Matsumoto, K.; Kuroki, N.; Numa, M.; Sebe, H.; Matsuzuka, R. A 34-mV Startup Ring Oscillator Using Stacked Body Bias Inverters for Extremely Low-Voltage Thermoelectric Energy Harvesting. In Proceedings of the 2020 18th IEEE International New Circuits and Systems Conference (NEWCAS), Montreal, QC, Canada, 16–19 June 2020.
65. Matsuzuka, R.; Terada, T.; Matsumoto, K.; Kitamura, M.; Hirose, T. A 42 mV startup ring oscillator using gain-enhanced self-bias inverters for extremely low voltage energy harvesting. *Jpn. J. Appl. Phys.* **2020**, *59*, SGGL01. [CrossRef]
66. Xie, Z.; Zhang, W.; Zhou, Q.; Wang, Y.; Wu, J.; Gou, J.; Liu, L.; Wang, Z.; Cai, Z. A high-efficiency power management unit with wide dynamic range for RF energy harvesting system. *IET Power Electron.* **2023**, *16*, 1293–1304. [CrossRef]
67. Chen, P.H.; Zhang, X.; Ishida, K.; Okuma, Y.; Ryu, Y.; Takamiya, M.; Sakurai, T. An 80 mV Startup Dual-Mode Boost Converter by Charge-Pumped Pulse Generator and Threshold Voltage Tuned Oscillator With Hot Carrier Injection. *IEEE J. Solid-State Circuits* **2012**, *47*, 2554–2562. [CrossRef]
68. Ma, Y.; Zou, Y.; Zhang, S.; Fan, X. A 50 mV Fully-Integrated Self-Startup Circuit for Thermal Energy Harvesting. *J. Circuits Syst. Comput.* **2017**, *26*, 1750196. [CrossRef]
69. Yu, X.; Lin, P.W.; Hsu, C.Y.; Yadav, S.K.; Lo, Z.J.; Peng, S.Y. An Integrated Circuit of A Cold-start-up Circuit for A Thermoelectric Energy Harvesting System. In Proceedings of the 2023 IEEE International Symposium on Circuits and Systems (ISCAS), Monterey, CA, USA, 21–25 May 2023; pp. 1–4.
70. Li, S.; Liu, X.; Calhoun, B.H. A 32nA Fully Autonomous Multi-Input Single-Inductor Multi-Output Energy-Harvesting and Power-Management Platform with 1.2×10^5 Dynamic Range, Integrated MPPT, and Multi-Modal Cold-start-Up. In Proceedings of the 2022 IEEE International Solid- State Circuits Conference (ISSCC), San Francisco, CA, USA,, 20–26 February 2022; Volume 65, pp. 1–3.
71. Coustans, M.; Krummenacher, F.; Kayal, M. A fully integrated 60 mV cold-start circuit for single coil DC-DC boost converter for Thermoelectric Energy Harvesting. *IEEE Trans. Circuits Syst. II Express Briefs* **2019**, *66*, 1668–1672. [CrossRef]
72. Dotche, K.A.; Salami, A.A.; Kodjo, K.M.; Sekyere, F.; Bedja, K.S. Artificial Neural Network Approach for the Integration of Renewable Energy in Telecommunication Systems. In Proceedings of the 2019 IEEE PES/IAS PowerAfrica, Abuja, Nigeria, 20–23 August 2019; IEEE: Piscataway, NJ, USA, 2019.
73. Breesam, W.I. Real-time implementation of MPPT for renewable energy systems based on Artificial intelligence. *Int. Trans. Electr. Energy Syst.* **2021**, *31*, e12864. [CrossRef]
74. Wang, X.; Xia, Y.; Zhu, Z.; Shi, G.; Xia, H.; Ye, Y.; Liu, L. Configurable hybrid energy synchronous extraction interface with serial stack resonance for multi-source energy harvesting. *IEEE J. Solid-State Circuits* **2022**, *58*, 451–461. [CrossRef]
75. Bakytbekov, A.; Nguyen, T.Q.; Li, W.; Lee Cottrill, A.; Zhang, G.; Strano, M.S.; Salama, K.N.; Shamim, A. Multi-source ambient energy harvester based on RF and thermal energy: Design, testing, and IoT application. *Energy Sci. Eng.* **2020**, *8*, 3883–3897. [CrossRef]
76. Lim, S.M.; Islam, M.S.; Sawal, M.A.; Razak, Z.; Yeo, K.H.; Wong, H.Y. Sub-threshold start-up circuit with dynamic body-biasing for boost converters in thermoelectric energy harvesting. *Sādhanā* **2020**, *45*, 149. [CrossRef]
77. Tao, J.; Mao, W.; Luo, Z.; Zeng, L.; Heng, C.H. A fully integrated power converter for thermoelectric energy harvesting with 81% peak efficiency and 6.4-mV minimum input voltage. *IEEE Trans. Power Electron.* **2021**, *37*, 4968–4972. [CrossRef]

Disclaimer/Publisher's Note: The statements, opinions and data contained in all publications are solely those of the individual author(s) and contributor(s) and not of MDPI and/or the editor(s). MDPI and/or the editor(s) disclaim responsibility for any injury to people or property resulting from any ideas, methods, instructions or products referred to in the content.